Journal of ELECTRONIC MATERIALS, Vol. 46, No. 11, 2017
DOI: 10.1007/s11664-017-5715-2

Influence of Sodium Chloride Doping on Thermoelectric Properties of *p*-type SnSe

SHI DAN YANG,[1] RAYMOND KWESI NUTOR,[1] ZI JIE CHEN,[1]
HAO ZHENG,[1] HAI FEI WU,[2] and JIAN XIAO SI[1,3]

1.—Department of Physics, Zhejiang Normal University, Jinhua 321004, People's Republic of China. 2.—Department of Physics, Shaoxing University, Shaoxing 312000, People's Republic of China. 3.—e-mail: sjx@zjnu.cn

We investigated the effect of NaCl doping on the thermoelectric properties of *p*-type $Sn_{1-x}Na_xSeCl_x$ (x = 0, 0.005, 0.01, 0.02, 0.03 and 0.04) prepared by a method which combines rapid induction melting and rapid hot pressing. After introducing the NaCl into the SnSe system, the carrier concentration of SnSe is significantly increased from $\sim 4.55 \times 10^{17}$ cm^{-3} to $\sim 3.95 \times 10^{19}$ cm^{-3} at 300 K. An electrical conductivity of $\sim$102.5 S cm^{-1} was obtained at 473 K by addition of 2 mol.% NaCl. It was found that Cl was effective in reducing the thermal conductivity by inducing abundant defects. A maximum ZT value of 0.84 was achieved in the $Na_{0.005}Sn_{0.995}SeCl_{0.005}$ sample at 810 K. This suggests that doping with NaCl is a facile and cost-effective method in optimizing the thermoelectric properties of SnSe materials.

Key words: Tin selenide, sodium chloride, thermoelectric performance

INTRODUCTION

Thermoelectric materials, which can directly convert heat energy into electrical power and vice versa, have attracted significant attention.[1,2] The performance of thermoelectric materials is characterized by a dimensionless figure-of-merit (ZT), defined as ZT = $(S^2\sigma/\kappa)T$, where S, σ, κ and T are the Seebeck coefficient, electrical conductivity, total thermal conductivity and the absolute temperature, respectively.[3] To optimize the electrical properties, chemical doping is a common and often-employed approach to modify the band structure. However, the chemical interaction between dopants and host matrix is complicated and is extremely difficult to control, which leads to the serious irreproducibility problem in the thermoelectric performance. SnSe, as a new promising thermoelectric material, suffers such inconsistency in the literature data due to the intricate defect formation.[4–7] As the best efficiency *p*-type dopants, alkali metals (Na, K atoms) would occupy Sn sites and contribute one hole to the valence band. But the electrical properties of SnSe are directly affected by the structural defects as well as the actual occupancy type of these dopants. Chen et al.[5] reported that the potassium doping in SnSe has dual effects that can simultaneously increase the carrier concentration and diminish Sn oxides. Zhang et al.[7] revealed that the introduction of Na into SnSe generated lamella-shaped defects and elemental segregation, which inevitably resulted in the deterioration of thermoelectric performance. It remains unsettled how the alkali-ions affect the electrical and thermal properties of SnSe, because the exact doping mechanism of SnSe by Na or K metal is unclear. In this work, the doping contribution of NaCl in SnSe to thermoelectric properties was investigated. To the best of our knowledge, no studies to date have investigated the effect of double substitution at Sn and Se sites. We show that Na and Cl co-doping results in an increase in electrical conductivity and a decrease in thermal conductivity, leading to a peak ZT value of $\sim$0.84 at 810 K. For a practical selection, NaCl provides a potential and cost-effective strategy for commercial SnSe thermoelectric devices.

(Received May 10, 2017; accepted July 17, 2017;

EXPERIMENTAL

Elemental Sn and Se powders supplied by Alfa Aesar, both with a purity of 99.999%, were used as starting materials in this study. The weighted composition of Sn, Se and NaCl (99%) were mixed and loaded into quartz tubes, which were vacuum evacuated and sealed. The quartz tubes were heated up to ~800°C in 10 min by an induction furnace, held for 10 min, and then naturally cooled to room temperature. The obtained ingots were ground into fine powder by hand and subsequently were sintered by the rapid hot pressing method (RHP) at a pressure of 50 MPa and temperature ~823 K for 5 min with a heating rate of ~110 K/min. The sintered pellets were polished and cut into coin-shaped samples of 2 mm in thickness and 10 mm in diameter. The phase structure was analyzed by powder x-ray diffraction (XRD) with Cu-Kα radiation (λ = 1.54178 Å). The chemical composition of the bulk samples was studied by an x-ray photo-electron spectroscope (XPS, PHI-5400, America). Fractured and polished surfaces of samples were examined by a field emission scanning microscope (FESEM, Hitachi, S-4800). Microstructures were observed by a high-resolution transmission electron microscope (HRTEM, JEM-2100F).

The Seebeck coefficient and electrical conductivity were measured simultaneously using a home-built system from room temperature to 810 K, and the uncertainty was 5% compared with commercial ZEM-3. The homebuilt device contains a vacuum chamber with a residual pressure of 10^{-2} Torr. The electrical conductivity (σ) was measured by the standard four-probe method and the Seebeck coefficient was obtained from the slope of the thermo-electromotive force and the temperature difference (~10 K) using Chromel–Niobium thermocouples. The Hall coefficient was tested by the Van der Pauw technique with a HMS-3000 system. The thermal diffusivity coefficient (λ) was measured by the laser flash method (Netzsch LFA-427). Thermal analysis was carried out using a differential scanning calorimeter (DSC, Netzsch STA 4495F). The heat capacity (C_p) was taken from reference.[4,8] The relative density (d) was measured using the conventional Archimedes principle and was over 96% of the theoretical density. The total thermal conductivity (κ) was calculated from $\kappa = \lambda C_p d$. We estimated an uncertainty of ±10% in the Seebeck coefficient and electrical conductivity measurements and ±8% in the thermal conductivity by considering the uncertainties for the thermal diffusivity, the specific heat, and the density. Therefore, the combined uncertainty for all measurements involved in ZT was estimated to be 15–20%.

RESULTS AND DISCUSSION

Phase and Microstructure

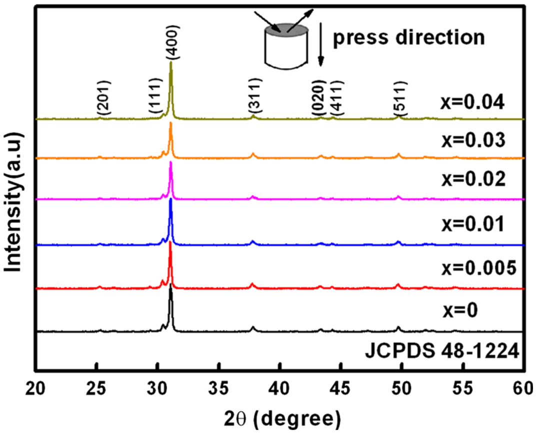

Fig. 1. Powder x-ray diffraction patterns of the $Na_xSn_{1-x}SeCl_x$ (x = 0, 0.005, 0.01, 0.02, 0.03 and 0.04) samples.

Powder x-ray diffraction patterns of the $Na_xSn_{1-x}SeCl_x$ (x = 0, 0.005, 0.01, 0.02, 0.03 and 0.04) samples are shown in Fig. 1. All diffraction peaks can be well indexed to the orthorhombic SnSe phase with the Pnma space group (PDF # 48-1224). The calculated lattice parameters (a = 11.513 Å, b = 4.155 Å, c = 4.452 Å) are in good agreement with literature data.[9–11] The strongest peak in (400) exhibits some preferred orientation perpendicular to the pressing direction. The peak positions (400) for $Na_xSn_{1-x}SeCl_x$ of x = 0.005, 0.01 and 0.02 slightly shift to a higher angle relative to the undoped sample due to the substitution of larger Sn and Se atoms by smaller atoms of Na and Cl. For NaCl-doping levels of x = 0.03 and 0.04, the peak positions did not change any more because of the doping limit of NaCl, as shown in Fig. S1 of the ESI. No second phase was observed within the detection limit of the x-ray. XPS measurements were performed for $Na_{0.04}Sn_{0.96}SeCl_{0.04}$ samples, as shown in Fig. 2a, b, c, and d. The Sn $3d_{3/2}$ and $3d_{5/2}$ orbital peaks were centered at 494.0 eV and 485.6 eV, respectively, and the Se $3d$ orbital peak at 53.5 eV. No obvious peaks for tin or selenium oxide were observed. Furthermore, the Na $1s$ and Cl $2p$ core level spectra are observed, confirming the presence of sodium and chlorine in the SnSe lattice.

The microstructure of $Na_{0.02}Sn_{0.98}SeCl_{0.02}$ samples was further characterized by SEM and TEM. As shown in Fig. 3a, the SEM image exhibits a lamellar microstructure, which is attributed to the van der Waals interaction of the bonds between adjacent layers. Typical lamellar domains stack together close with tens of microns in size which contain many thin layers of the same orientation. HRTEM revealed two kinds of representative microstructures in the sample. First, heavily distorted lattices in the matrix are shown in Fig. 3b. Next, Fig. 3c shows the existence of the abundant nanoprecipitates, which created a large amount of interlacing grain boundaries. The measured interplanar distance of d = 0.292 nm/0.336 nm closely matched the standard value of 0.293 nm/0.336 nm for the lattice plane (111)/(210) of the SnSe

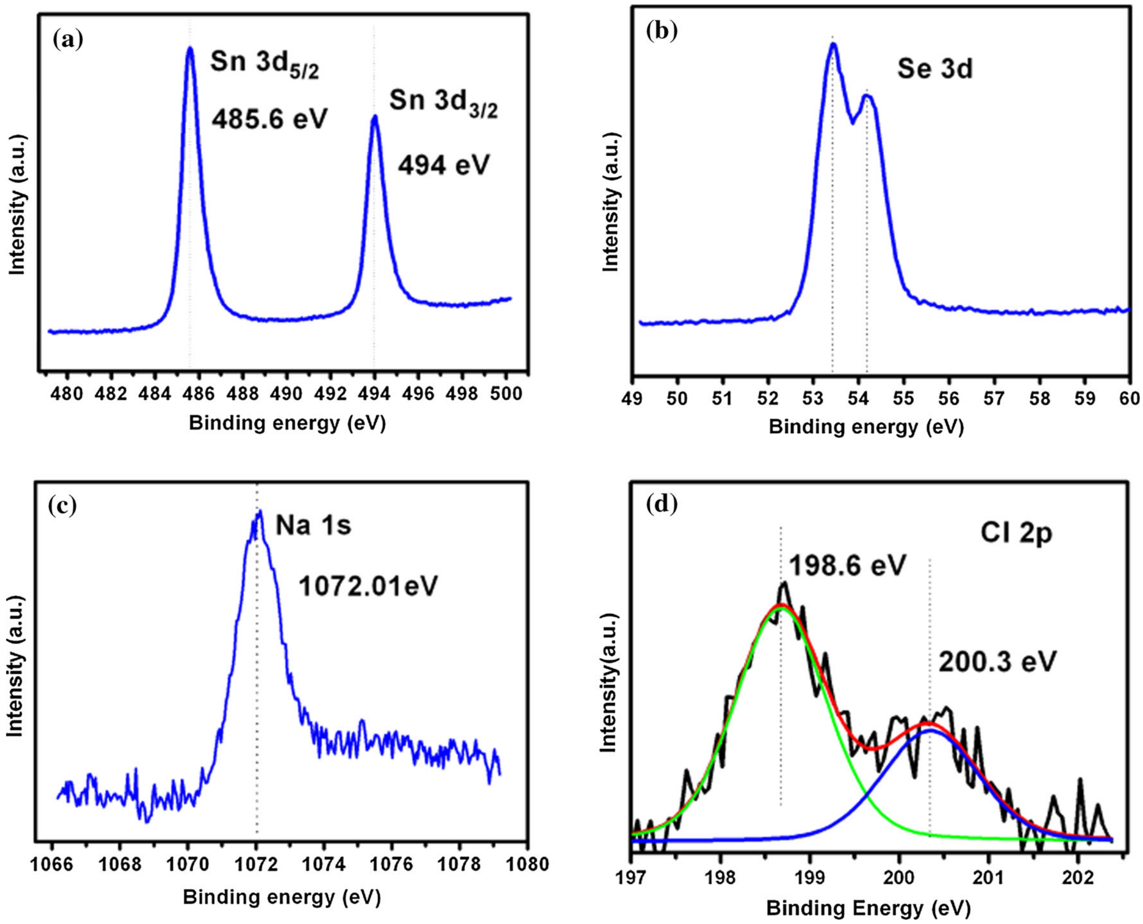

Fig. 2. (a–d) XPS spectra of the $Na_{0.04}Sn_{0.96}SeCl_{0.04}$ sample for Sn (3*d*), Se(3*d*), Na(1*s*) and Cl (2*p*), respectively.

orthorhombic phase. Fig. S2 in ESI shows the HRTEM image for the undoped SnSe. Versus the $Na_{0.02}Sn_{0.98}SeCl_{0.02}$ sample shown in Fig. 3b and c, the differences in the microstructure can be observed. The grain size e is smaller and the numbers of defects are more pervasive after the NaCl doping. The multiple defects are attributed to the high mass fluctuations between the dopant NaCl to the host SnSe (118.69, 78.96, 22.99 and 35.45 amu for Sn, Se, Na and Cl, respectively). Moreover, the large ionic radius mismatch between the dopant Cl^- (181 pm) and Se^{2-} (198 pm) at the anion site give rise to the increase of defect density in the materials,[12,13] which might be beneficial for the reduction of thermal conductivity via phonon scattering.

EIECTRICAL AND THERMAL TRANSPORT PROPERTIES

Figure 4a shows the electrical transport properties as a function of temperature for all samples. The electrical conductivity for the pristine SnSe remains at a low value of ~1.6 S cm^{-1} below 573 K, then rapidly increases to 14.17 S cm^{-1} at 773 K, showing typical semiconducting behavior. Similar properties were also previously reported in undoped polycrystalline SnSe.[9,10] After doping with NaCl, the electrical conductivity rapidly increased from 1.1 S cm^{-1} for $x = 0$ S cm^{-1} to 41.36 S cm^{-1} for $x = 0.005$ at 300 K. For all the NaCl doped samples, the electrical conductivity is initially significantly increased, then turns to decrease at 500 K, but finally increases again over 723 K with temperature. The anomaly in electrical transport around 300–500 K was also observed in Na-doped $SnSe_{1-x}Te_x$ polycrystals and the isostructural SnS prepared by mechanical alloying and spark plasma sintering, and was ascribed to the effect of energy barrier scattering at grain boundaries.[14–18] A maximum electrical conductivity of ~102.5 S cm^{-1} for the sample of $x = 0.02$ was obtained at 473 K, which is 85 times higher than pure SnSe (1.2 S cm^{-1}) and also far higher than that of Na-doped[9,19] and Ag-doped[10,20] polycrystalline SnSe as well as comparable to the reported values of highly textured samples at the same temperature point.[18,21]

The significant enhancement of the electrical conductivity is attributed to the increment of the carrier concentration. As seen in Table I, the sign of the Hall coefficient is positive for all samples, which indicates a *p*-type conduction behavior. The Hall

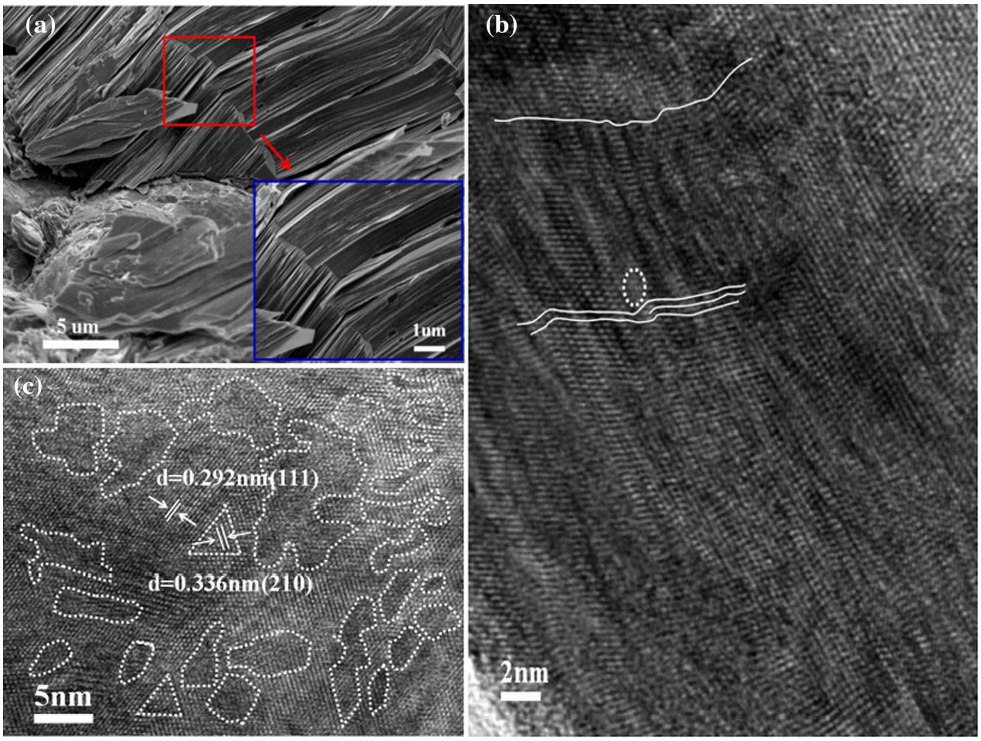

Fig. 3. (a) SEM image of the freshly fractured surface of $Na_{0.02}Sn_{0.98}SeCl_{0.02}$ sample. HRTEM images of $Na_{0.02}Sn_{0.98}SeCl_{0.02}$ samples: (b) heavily distorted lattices in the matrix; (c) existence of the abundant nanoprecipitate, which created a large amount of interlacing grain boundaries.

carrier concentration of pristine SnSe is around 4.55×10^{17} cm^{-3} at 300 K and greatly enlarged by two orders after doping with NaCl to 3.95×10^{19} cm^{-3} for $x = 0.005$ sample. It is known that the Sn vacancy acts as a two-electron acceptor and the Na substitution in Sn-site introduces a single hole into the system.[22] Meanwhile, the Cl occupied at the Se-site should act as a single donor and counterbalance the increase of hole concentration. However, in our case, a slight excess of Se was used to compensate the Se evaporation and mitigate the formation of Se vacancy defects in $Na_xSn_{1-x}SeCl_x$ samples. Under such a Se-rich condition, the formation enthalpy of Cl_{Se} defect may be larger than that of the Na_{Sn} defect. The concentration of Na_{Sn} defect surpasses that of Cl_{Se}, which introduces extra holes in the $Na_xSn_{1-x}SeCl_x$ sample. The Na_{Sn} acceptor and intrinsic Sn vacancy occur simultaneously, making the hole concentration increase significantly. With increasing NaCl content ($x \geq 0.01$), the concentration of holes is somewhat decreased. The reason for this may be either an increase of the defect formation enthalpy for Sn vacancy in the presence of Cl doping or the self-compensation of Cl_{Se} defect gradually becomes dominate.

Figure 4b shows the temperature dependence of the Seebeck coefficient for $Na_xSn_{1-x}SeCl_x$ (x = 0, 0.005, 0.01, 0.02, 0.03 and 0.04) samples. For the $x = 0$, the Seebeck coefficient is 478.93 μV K^{-1} at 300 K and increases to 522.03 μV K^{-1} at 523 K, then it starts to decrease with increasing temperature due to the bipolar effect of minority carrier excitation. After doping with NaCl, the Seebeck coefficient gradually decreases from 478.93 μV K^{-1} for $x = 0$ μV K^{-1} to 121.8 μV K^{-1} for $x = 0.04$, and the trend of the Seebeck coefficient variation for the samples of $x > 0$ shows similar behavior with increasing temperature and is almost consistent in the range from 300 K to 810 K. Combined with excellent electrical conductivity and moderate Seebeck coefficient, the doped samples show a significantly enhanced power factor (PF), as shown in Fig. 4c. A maximum PF of ~4.14 μW cm^{-1} K^{-2} is obtained for $x = 0.005$ at 810 K, which is two times higher than that of the SnSe pristine sample (~1.83 μW cm^{-1} K^{-2}). After introducing the NaCl, the power factor of samples of $x < 0.02$ show significant improvement in a relatively wide mid-temperature range (300–700 K).

Figure 4d shows the temperature dependence of the total thermal conductivity (κ_{tol}) of $Na_xSn_{1-x}SeCl_x$ (x = 0, 0.005, 0.01, 0.02, 0.03 and 0.04). The total thermal conductivities of all samples decrease with increasing temperature. For $x = 0.005$ sample, the total thermal conductivity value is ~1.11 Wm^{-1} K^{-1} at 298 K, and it reaches ~0.39 Wm^{-1} K^{-1} at 810 K. The lattice thermal conductivity (shown in Fig. 4e) is calculated using $\kappa_{\mathrm{lat}} = \kappa_{\mathrm{tol}} - \kappa_{\mathrm{ele}}$. The electronic contribution can be evaluated by the Wiedemann–Franz law, $\kappa_{\mathrm{ele}} = L\sigma T$, where an L of 1.49×10^{-8} V^2 K^{-2} is

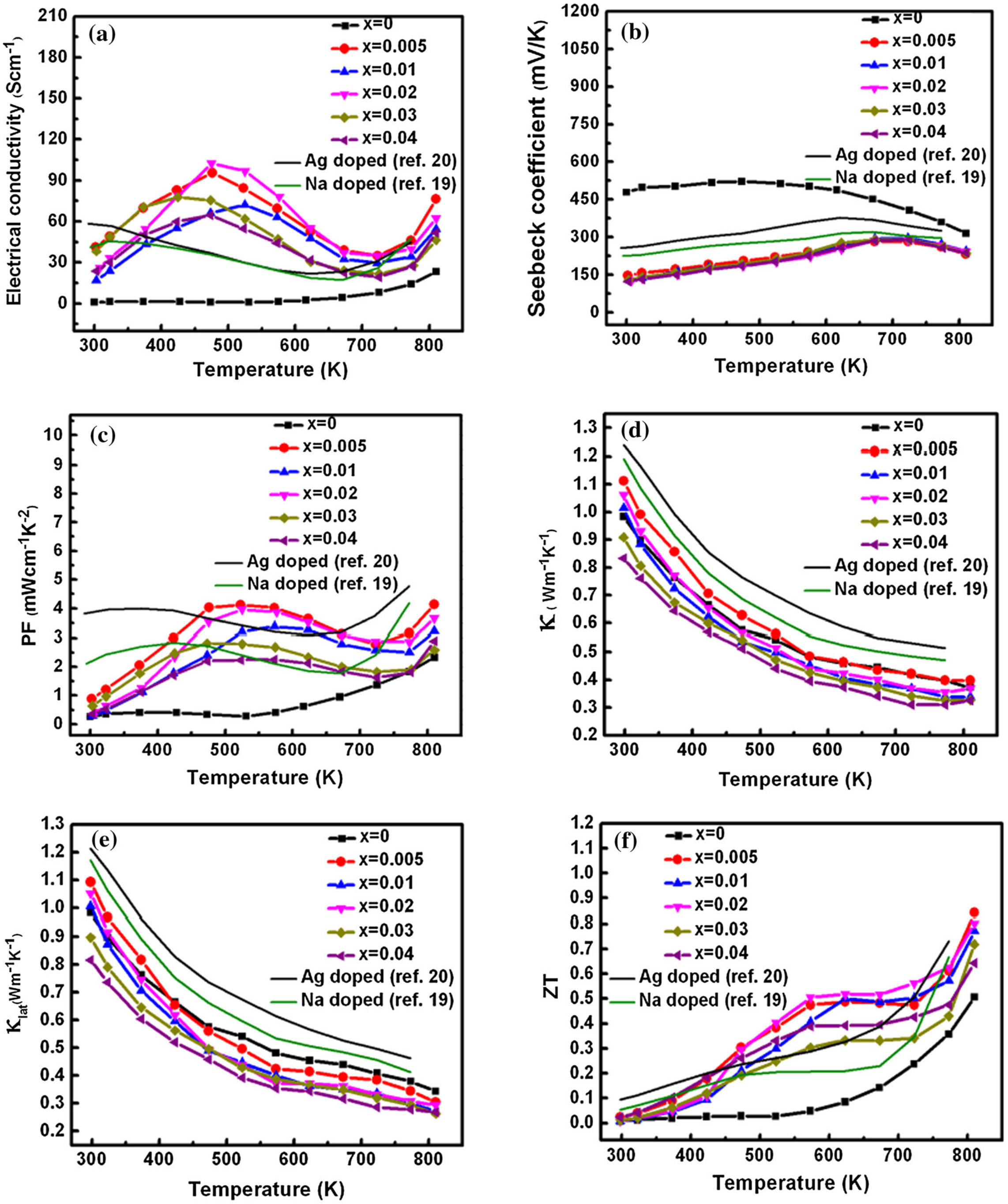

Fig. 4. Temperature dependence of (a) electrical conductivity, (b) Seebeck coefficient, (c) power factor, (d) total thermal conductivity, (e) lattice thermal conductivity and (f) figure of merit ZT for $Na_xSn_{1-x}SeCl_x$ (x = 0, 0.005, 0.01, 0.02, 0.03 and 0.04) samples.

obtained by fitting the Seebeck data to the reduced chemical potential.[21] Above 473 K, the lattice thermal conductivity of all samples is lower than that of the pristine SnSe. For $x = 0.005$, the κ_{lat} is 1.09 Wm^{-1} K^{-1} then reduced to 0.81 Wm^{-1} K^{-1} in a $x = 0.04$ sample. The lowest κ_{lat} value is ~0.27 Wm^{-1} K^{-1} for $x = 0.04$ at 810 K, which is close to that of single-crystal SnSe.[4,23] Here, we noticed that the κ_{tol} of the Na single doped sample is larger than that of the un-doped sample, which is due to the scattering of the phonons weakened by the substitution of Na^+ for Sn^{2+} in the cation site.[4,24] However, the presence of Cl in SnSe leads to a decrease in total thermal conductivity. The κ_{tol} values of co-doped samples decrease with the increase of NaCl content. This suggests that the introduction of the amount of Cl should be attributed to the decrease of the thermal conductivity. The reason for this may be an

Table I. Room temperature Hall carrier concentrations, and density of the $Na_xSn_{1-x}SeCl_x$ (x = 0, 0.005, 0.01, 0.02, 0.03 and 0.04) samples

Nominal composition $Na_xSn_{1-x}SeCl_x$	Density (g cm^{-3})	Carrier density (10^{19} cm^{-3})
0	6.11	0.045
0.005	6.05	3.95
0.01	6.05	3.27
0.02	5.94	2.71
0.03	5.99	2.59
0.04	6.03	2.46

enhancement of phonon scattering in the presence of Cl due to the multiple defects formation at the nanoscale level, as shown in Fig. 3b and c. Such defects induced by Cl doping were also observed in NaCl co-doped PbTe[25] and Cl doped nanostructured $AgPb_{18}SbSe_{20}$.[26]

Figure 4f presents the temperature dependence of the ZT value for all samples. In contrast to a Na single doped sample, the ZT values of co-doped samples were significantly enhanced in a wide temperature range from 500 K to 700 K due to the optimized electrical and thermal transport properties. A maximum ZT value of 0.84 was achieved for the sample of $x = 0.005$ at 810 K, which is 68% higher than that (0.5) of the un-doped polycrystalline SnSe compound. Based on measurements of the areas under the curves of Fig. 4f, the average ZT of 0.35 from 300 K to 773 K was obtained for the $Na_{0.005}Sn_{0.995}SeCl_{0.005}$ sample. This is higher than the results reported of Ag-doped SnSe ($ZT_{ave} \approx 0.27$)[10,20] and Na-doped SnSe ($ZT_{ave} \approx 0.32$).[9,19] This suggests that the NaCl is a quite effective dopant in optimizing the thermoelectric properties of SnSe materials.

CONCLUSIONS

In summary, polycrystalline SnSe doped with NaCl was prepared by rapid induction melting followed by rapid hot pressing (RMP). The NaCl dopant enhances the carrier concentration and electrical conductivity of SnSe. A maximum power factor of $\sim$4.14 μW cm^{-1} K^{-2} was obtained at 810 K. The presence of Cl in SnSe contributes to a low lattice thermal conductivity of $\sim$0.27 Wm^{-1} K^{-1} at 810 K. As a result, a peak ZT value of 0.84 was obtained at 810 K for the $Na_{0.005}Sn_{0.995}SeCl_{0.005}$ sample. These findings suggest that the cost-effectiveness of NaCl provides a quite practical strategy to optimize the thermoelectric properties of polycrystalline SnSe, which is more commercially available for TE device fabrication than that of expensive silver and unstable sodium.

ACKNOWLEDGEMENTS

This work was supported by the National Natural Science Foundation of China (Grant Nos. 51302248 and 51202149), Zhejiang Provincial Natural Science Foundation of China (Grant No. Y1110563).

ELECTRONIC SUPPLEMENTARY MATERIAL

The online version of this article (doi: 10.1007/s11664-017-5715-2) contains supplementary material, which is available to authorized users.

REFERENCES

1. Y. Pei, X. Shi, A. LaLonde, H. Wang, L. Chen, and G.J. Snyder, *Nature* 473, 66 (2011).
2. K. Biswas, J. He, I.D. Blum, C.I. Wu, T.P. Hogan, D.N. Seidman, V.P. Dravid, and M.G. Kanatzidis, *Nature* 489, 414 (2012).
3. J.P. Heremans, V. Jovovic, E.S. Toberer, A. Samarat, K. Kurosaki, A. Charoenphakdee, S. Yamanaka, and G.J. Snyder, *Science* 321, 554 (2008).
4. L.D. Zhao, G. Tan, S. Hao, J. He, Y. Pei, H. Chi, H. Wang, S. Gong, H. Xu, V.P. Dravid, C. Uher, G.J. Snyder, C. Wolverton, and M.G. Kanatzidis, *Science* 351, 141 (2016).
5. Y.X. Chen, Z.H. Ge, M. Yin, D. Feng, X.Q. Huang, W. Zhao, and J. He, *Adv. Funct. Mater.* 26, 6836 (2016).
6. L.D. Zhao, C. Chang, G. Tan, and M.G. Kanatzidis, *Energy Environ. Sci.* 9, 3044 (2016).
7. B. Zhang, K. Peng, A. Li, X. Zhou, Y. Chen, Q. Deng, and X. Han, *J. Alloys. Compd.* 688, 1088 (2016).
8. S.I. Kim, K.H. Lee, H.A. Mum, H.S. Kim, S.W. Hwang, J.W. Roh, D.J. Yang, W.H. Shin, X.H. Li, Y.H. Lee, G.J. Snyder, and S.W. Kim, *Science* 348, 109 (2015).
9. E.K. Chere, Q. Zhang, K. Daha, F. Cao, J. Mao, and Z. Ren, *J. Mater. Chem. A* 4, 1848 (2016).
10. C.L. Chen, H. Wang, Y.Y. Chen, T. Daya, and G.J. Snyder, *J. Mater. Chem. A* 2, 11171 (2014).
11. Q. Zhang, E.K. Chere, J. Sun, F. Cao, K. Dahal, S. Chen, G. Chen, and Z. Ren, *Adv. Energy Mater.* 5, 1500360 (2015).
12. Z. Zhou, X. Tan, G. Ren, Y. Lin, and C. Nan, *J. Electron. Mater.* 46, 2593 (2017).
13. G. Tan, L.D. Zhao, and M.G. Kanatzidis, *Chem. Rev.* 116, 12123 (2016).
14. T.R. Wei, C.F. Wu, X. Zang, Q. Tan, L. Sun, Y. Pan, and J.F. Li, *Phys. Chem. Chem. Phys.* 17, 30102 (2015).
15. Q. Tan, L.D. Zhao, J.F. Li, C.F. Wu, T.R. Wei, Z.B. Xing, and M.G. Kanatzidis, *J. Mater. Chem. A* 2, 17302 (2014).
16. T.R. Wei, G. Tan, X. Zhang, C.F. Wu, J.F. Li, V.P. Dravid, G.J. Snyder, and M.G. Kanatzidis, *J. Am. Chem. Soc.* 138, 8875 (2016).
17. Y. Zheng, S. Wang, W. Liu, Z. Yin, H. Li, X. Tang, and C. Uher, *J. Phys. D Appl. Phys.* 47, 115303 (2014).
18. Y. Li, F. Li, J. Dong, Z. Ge, F. Kang, J. He, H. Du, B. Li, and J.F. Li, *J. Mater. Chem. C* 4, 2047 (2016).

19. H.Q. Leng, M. Zhou, J. Zhao, Y.M. Han, and L.F. Li, *RSC Adv.* 6, 9112 (2016).
20. H. Leng, M. Zhou, J. Zhao, Y.M. Han, and L.F. Li, *J. Electron. Mater.* 45, 527 (2016).
21. Y. Fu, J. Xu, G.Q. Liu, J. Yang, X. Tan, Z. Liu, H. Qin, H. Shao, H. Jiang, B. Liang, and J. Jiang, *J. Mater. Chem. C* 4, 1201 (2016).
22. A. Dewandre, O. Hellman, S. Bhattacharya, A.H. Romero, G.K.H. Madsen, and M.J. Verstraete, *Phys. Rev. Lett.* 117, 276601 (2016).
23. L.D. Zhao, S.H. Lo, Y. Zhang, H. Sun, G. Tan, C. Uher, C. Wolverton, V.P. Dravid, and M.G. Kanatzidis, *Nature* 508, 373 (2014).
24. K. Peng, X. Lu, H. Zhan, S. Hui, X. Tang, G. Wang, J. Dai, C. Uher, G. Wang, and X. Zhou, *Energy Environ. Sci.* 9, 454 (2016).
25. I. Cohen, M. Kaller, G. Komisarchik, D. Fuks, and Y. Gelbstein, *J. Mater. Chem. C* 3, 9559 (2015).
26. Q. Zhang, Y. Lan, S. Yang, F. Cao, M. Yao, C. Opeil, D. Broido, G. Chen, and Z. Ren, *Nano Energy* 2, 1121 (2013).